Supporting Information

del Jesus et al. 10.1073/pnas.1218636109

SI Materials and Methods

Maximizing Ecosystem Productivity. The Upper Rio Salado river basin (URS) is discretized by means of a spatial square grid, with pixel side length of 1 arc-second (28.5 m on average). Pixels are homogeneous subdivisions where climatic conditions, soil texture, and colonizing vegetation type characterize productivity (productivity, assimilation, and canopy photosynthesis are synonyms in this paper). The bulk of productivity takes place during the growing season (1). A stochastic implementation of the water balance at the pixel scale is used to deal with the intrinsic variability of the system drivers constraining photosynthesis. The productivity of the ecosystem is defined as the sum of the productivity of every pixel of the URS. The optimization of ecosystem productivity is achieved by modifying the functional vegetation type that occupies every pixel of the domain (keeping climatic conditions and soil texture constant).

We assume that to study the large-scale vegetation patterns in the URS, the interaction among pixels may be omitted; i.e., the lateral redistribution of soil moisture is negligible, which is a reasonable assumption in semiarid environments like the URS. This assumption ensures a global optimum exists, the optimum being independent of the initial state of the system. The overall optimum can thus be obtained by combining the local optima at every pixel of the basin.

The state reached by many natural systems, however close, may not be the optimum state, e.g., the maximum entropy production (MEP) state. This behavior is known as feasible optimality (2). The concept of feasible optimality accounts for all those factors that are not explicitly included in the analysis of a system, preventing the system from attaining its optimal state of operation. In this work the maximization of productivity is carried out via a simulated annealing procedure to account for feasible optimality.

When applied to the optimization of canopy photosynthesis, simulated annealing is carried out as follows. An initial state is assigned to the system, in our case a random vegetation organization in the basin (Fig. 2*D*). The annealing parameter is initially set to a large value for which the random vegetation distribution constitutes a steady state (θ larger than 1.0 in the URS). Then an iterative process is started. At every iteration, the vegetation type at a randomly chosen location is tentatively changed to a new vegetation type, randomly selected among the other possible ones potentially existing in the basin. The tentative change is accepted if it increments canopy photosynthesis, i.e., productivity or assimilation. In the case that it decreases assimilation, the change may be accepted with probability

$$p = e^{\frac{-|\Delta|}{\varphi\theta}},$$

where Δ is the absolute value of the change, φ is a constant of value 1 with units of assimilation, and θ is the dimensionless annealing parameter of the simulated annealing procedure. The larger the annealing parameter is, the more probable it is that a change will be accepted. Once a steady state for assimilation has been attained (it takes an average of 25 million iterations in the case of the URS), the annealing parameter is decreased and the process repeated until all of the parameters in the experiment schedule have been tested. As a result, the optimization process produces a steady-state solution for every different value of the annealing parameter of the system.

Isothermal Assumption. In the main text, to simplify the expression of the system's entropy production, it is assumed that the transformations are isothermal. This assumption implies that at a given location of the basin, the temperature at which photosynthesis and respiration take place is constant and independent of the type of vegetation populating the site. Thus, different rates of entropy production at a site become dependent only on the vegetation type controlling the carbon cycle at that site.

In any case, the contribution from temperature variations would be small. At the URS there exists a 1,000-m difference in elevation between the outlet and the highest point. This difference in elevation induces a difference in temperature of about 10 °C, that is, temperatures ranging approximately from 285 K (12 °C) to 295 K (22 °C). Therefore, the maximum difference introduced by temperature in the computation of entropy production would be about 3.5%.

Assimilation Computation. The relation between the flux of carbon dioxide entering the plant and the flux of water vapor lost to the atmosphere during the transpiration process may be measured by means of the water use efficiency (WUE). WUE is normally expressed in [mmol $CO_2 \cdot mol^{-1}$ H_2O]. Considering 1 mol of CO_2 is 44 g of CO_2, and 1 mol of H_2O is 18 g, WUE can be expressed in [g $CO_2 \cdot g^{-1}$ H_2O], multiplying by $(44/18) \times 10^{-3}$ (Table S1).

Transpiration times water use efficiency provides the mass of CO_2 fixed by square meter and day [kg $CO_2 \cdot d^{-1} \cdot m^{-2}$]. Multiplying by the surface area of a pixel, the total mass of CO_2 the pixel fixes daily is obtained. As only 18 g of carbon is present in the 44 g of carbon dioxide, the mass of CO_2 previously obtained is multiplied by (12/44) to obtain the amount of carbon fixed daily by the pixel considered.

The assimilation at every pixel is thus computed as the product of the average transpiration of the pixel (derived from the hydrologic model described later) and the WUE of the functional vegetation type populating the pixel.

Study Site and Input Data Description. The URS is located within the Sevilleta Long-Term Ecological Research (LTER) site, adjacent to the Cibola National Forest, New Mexico. It covers an area of 466 km^2 and presents elevations ranging from 1,985 m above mean sea level (a.s.l.) to 2,880 m a.s.l. It is a semiarid environment with a growing season from May to September.

A digital elevation model (DEM) for the basin with a resolution of 1 arc-second was obtained from the US Geological Survey National Elevation Dataset (3, 4). A 1-arc-second resolution map of soil texture distribution was obtained from the US Department of Agriculture (USDA) STATSGO soil database (5) (Fig. S1). Soil parameters are presented in Table S3.

Soil cover data were obtained from the 1-arc-second resolution US Geological Survey National Land Cover Dataset (6) (NLCD) derived from Landsat imagery (Fig. 2*A*). Soil cover data indicate the spatial distribution of different functional vegetation types in the basin, without distinction of species. Trees (*Pinyon–Juniper* woodland), shrubs (mainly *Larrea tridentata*), and grasses (Black Grama, *Bouteloua eriopoda*; and Blue Grama, *Bouteloua gracilis*) are the dominant species in the URS. Their key functional characteristics are shown in Table S2.

Data from six meteorological stations (7) (stations 40–45) with hourly records from 1987 to 2010 were used to characterize daily averages of rainfall, vapor pressure, relative humidity, air temperature, wind speed, and incoming shortwave solar radiation. Growing season averages were determined for every variable at every meteorological station. Rainfall is modeled as a marked Poisson process on a daily scale (2). It is characterized by two

parameters: the frequency of rainy days during the growing season, $\lambda[d^{-1}]$, and the average storm depth, α[mm], which is assumed to have an exponential distribution. λ and α are calculated for every station and a regression with the elevation of the station is obtained for each parameter. These regressions (shown below, where Z is elevation above mean sea level [m]) serve to downscale the rainfall parameters across the whole basin, assigning a λ- and an α-value to every pixel of the basin:

$$\lambda = 0.1077 + 6.75 \times 10^{-5} \cdot Z \quad R^2 = 0.586$$
$$\alpha = -1.649 + 0.0038 \cdot Z \quad R^2 = 0.835.$$

A regression was established by relating growing season average air temperature and two station variables: elevation and measured growing season average incoming shortwave solar radiation. The resulting regression is shown below, where Z is elevation above mean sea level [m] and SW_{inc} is incoming shortwave solar radiation $[J \cdot m^{-2} \cdot s^{-1}]$:

$$T_a = 27.6 - 0.0068Z + 0.0176 \cdot SW_{inc} \quad R^2 = 0.57.$$

At every pixel the above regression requires SW_{inc} values to compute air temperature. A daily incoming shortwave radiation (ISR) is modeled for every pixel of the basin, using the r.sun (8) module of the GRASS GIS software (9). ISR calculation accounts for pixel location, aspect, and shading effects. A growing season average for ISR is calculated by averaging the values at mid-May, mid-June, and mid-August. A dimensionless coefficient (k_{ISR}) is defined at every pixel by dividing its growing season average ISR value by the growing season ISR basin average (Fig. S2). The growing season average SW_{inc} for every pixel of the basin is computed multiplying its k_{ISR} by the growing season average incoming shortwave solar radiation, computed for the whole basin from the measured values at the meteorological stations.

Hydrologic Modeling. The hydrologic modeling at the daily scale is based in the full computation of the stochastic water balance at every pixel through the probability density function (pdf) of soil moisture (10, 11). In the modeling scheme evapotranspiration is assumed to be an increasing function of soil moisture, ranging from zero, for soil moisture values below the hygroscopic point, to a maximum at the potential evapotranspiration (PET), when soil moisture reaches values larger than those corresponding to incipient stomata closure.

The wilting point and the soil moisture corresponding to incipient stomata closure are functions of soil texture and plant type. PET is evaluated by means of the Penmann–Monteith model and depends on climatic conditions and vegetation characteristics. For the computation of net radiation it is assumed that, at any given site, canopy and air temperatures are equal (12). Canopy conductance is evaluated as the product of the leaf area index and the maximum stomatal conductance. The aerodynamic atmospheric conductance is evaluated considering wind speed and plant dimensions. Vapor pressure and vapor pressure gradients are evaluated from meteorological data. PET is estimated at the daily scale, considering the average length of a day during the growing season at the URS.

The steady-state components of the water balance at the daily scale are solved by integrating the stochastic differential equation (SDE) of soil moisture (10, 11). A previous study in the URS (13) pointed out the importance of the initial condition of soil moisture at the start of the growing season to correctly evaluate the average value of the different components of the water balance at each site of the basin. The initial condition is controlled by the snowmelt accumulated in the soil at the beginning of the growing season. This initial condition creates an initial transient regime that is not captured by the steady-state soil moisture pdf. After this initial regime, the steady-state pdf is a valid representation of the physical processes taking place (11).

In this paper the initial soil moisture at each site at the start of the growing season is evaluated by accounting for the water equivalent of the snow (SWE) infiltrated into the soil. It is assumed that a site, i.e., a pixel, (*i*) located at the snow line, i.e., 2,300 m, (*ii*) colonized by tree vegetation, and (*iii*) presenting silt loam soil texture starts the growing season under saturation conditions. This assumption implies 502 mm of SWE must be present at the site. Above the snow line, a constant 502 mm SWE is assumed. Below it, an exponential decay is assumed, given by the equation

$$W = \widehat{W}\ e^{-k\left(\widehat{H}-z\right)},$$

where W is the SWE at elevation z, $\widehat{W}$ is the saturation SWE (502 mm), $\widehat{H}$ is the height of the snow line (2,300 m), and k is the decay constant (0.01).

The SWE so obtained is modified to account for the effect of site orientation, i.e., aspect. To this effect SWE is divided by the solar radiation coefficient k_{ISR} (Fig. S2). This operation increases SWE in shaded sites and reduces it in exposed sites. The initial soil moisture is then computed, assuming SWE is equally distributed over the volume of the soil pores, i.e., the product of average root depth and soil porosity.

The duration of the transient regime is evaluated by computing the mean first passage time (14) (MFPT) that the soil moisture takes to go from its initial value to the first descending cross below the threshold corresponding to incipient stomata closure.

During the transient regime plants evapotranspire at the potential rate (PET). Afterward, evapotranspiration is provided by the average steady-state solution. The growing season evapotranspiration is evaluated as a weighted average between evapotranspiration during the transient and that during the steady regimes (11), as expressed in the equation

$$\overline{ET}_{GS} = \frac{1}{T_{GS}}\{MFPT \cdot PET + (T_{GS} - MFPT) \cdot \overline{ET}_{SS}\},$$

where $\overline{ET}_{GS}$ is the average growing season evapotranspiration, $\overline{ET}_{SS}$ is the average steady-state evapotranspiration, and T_{GS} is the growing season length in days.

Average growing season transpiration is then evaluated by subtracting bare soil evaporation from the average growing season evapotranspiration. Bare soil evaporation is assumed constant and equal to α_s for the whole basin.

1. Caylor KK, Manfreda S, Rodriguez-Iturbe I (2005) On the coupled geomorphological and ecohydrological organization of river basins. *Adv Water Resour* 28:69–86.
2. Rodriguez-Iturbe I, Rinaldo A (1997) *Fractal River Basins. Chance and Self-Organization* (Cambridge Univ Press, Cambridge, UK).
3. Gesch D, et al. (2002) The National Elevation Dataset. *Photogramm Eng Remote Sensing* 68(1):5–11.
4. Gesch DB (2007) *The National Elevation Dataset. Digital Elevation Model Technologies and Applications: The DEM Users Manual*, ed Maune D (American Society for Photogrammetry and Remote Sensing, Bethesda), 2nd Ed, pp 99–118. Available at http://seamless.usgs.gov.
5. US Department of Agriculture, Service UNRC (1994) State soil geographic (statsgo) database, miscellaneous publication no. 1492. Available at http://soildatamart.ncrs.usda.gov. Accessed June 2012.
6. Vogelmann JE, et al. (2006) Completion of the 1990s national land cover data set for the conterminous United States from landsat thematic mapper data and ancillary data sources. *Photogramm Eng Remote Sensing* 67:650–652.
7. Moore DI (2010) *Meteorology Data at the Sevilleta National Wildlife Refuge, New* Mexico (Long-Term Ecological Research Network). Available at http://sev.lternet.edu/data/sev-12010. Accessed June 2012.
8. Hofierka J, Suri M (2002) The solar radiation model for Open source GIS: Implementation and applications. *Proceedings of the Open source GIS - GRASS Users Conference 2002*, eds Ciolli M, Zatelli P (Trento, Italy), pp 1–19.
9. GRASS Development Team (2012) *Geographic Resources Analysis Support System (GRASS), GNU General Public License*. Available at http://grass.osgeo.org. Accessed June 2012.

10. Laio F, Porporato A, Ridolfi L, Rodriguez-Iturbe I (2001) Plants in water-controlled ecosystems: Active role in hydrologic processes and response to water stress: II. Probabilistic soil moisture dynamics. *Adv Water Resour* 24:707–723.
11. Rodriguez-Iturbe I, Porporato A (2004) *Ecohydrology of Water-Controlled Ecosystems* (Cambridge Univ Press, Cambridge, UK).
12. Jones HG (1992) *Plants and Microclimate: A Quantitative Approach to Environmental Plant Physiology* (Cambridge Univ Press, Cambridge, UK).
13. Caylor KK, Scanlon TM, Rodriguez-Iturbe I (2004) Feasible optimality of vegetation patterns in river basins. *Geophys Res Lett* 31:L13502.
14. Laio F, Porporato A, Ridolfi L, Rodriguez-Iturbe I (2001) Mean first passage times of processes driven by white shot noise. *Phys Rev E Stat Nonlin Soft Matter Phys* 63(3 Pt 2):036105.

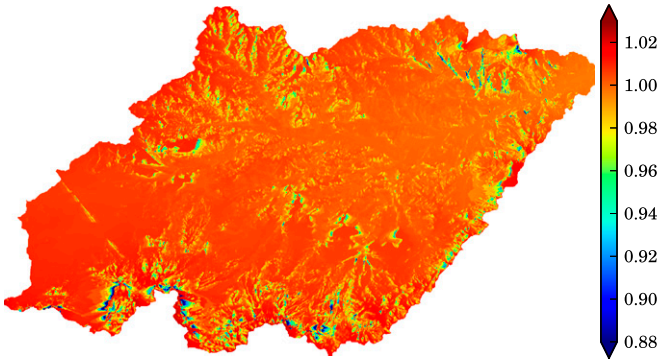

Fig. S1. Spatial distribution of k_{ISR}. Spatial distribution of the irradiation coefficient at the basin is shown. The coefficient accounts for relief shading effects.

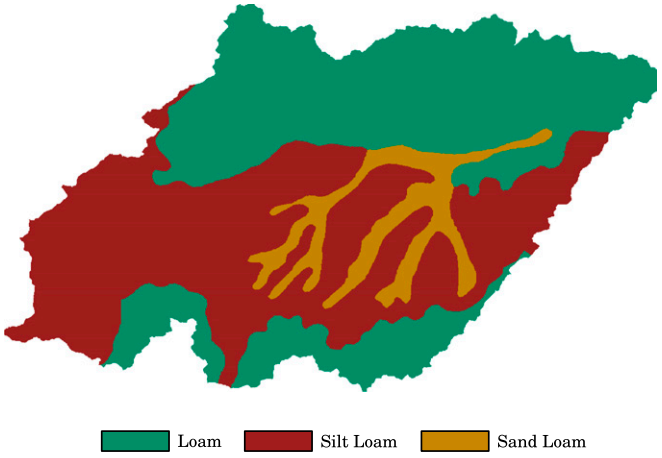

Fig. S2. Spatial distribution of the main three soil textures present at the upper Rio Salado basin.

Table S1. WUE values for the different plant species used in the simulations

Vegetation cover	WUE [mmol $CO_2 \cdot mol^{-1} H_2O$]	WUE [g $CO_2 \cdot g^{-1} H_2O$]
Pinyon–Juniper	5.84	14.27×10^{-3}
Larrea tridentata	8.40	20.53×10^{-3}
Bouteloua gracilis	4.10	10.02×10^{-3}
Bouteloua eriopoda	4.30	10.51×10^{-3}

The values are representative averages over the growing season. Tree data (*Pinyon–Juniper*) were provided by Jean-Marc Limousin, University of New Mexico. Shrub data (*Larrea tridentata*) were provided by Juliana Medeiros, University of Kansas. Grass data (*Bouteloua gracilis* and *Bouteloua eriopoda*) were provided by Michell L. Thomey, University of New Mexico.

Table S2. Vegetation parameters

Vegetation cover	Ψ_w [MPa]	Ψ^* [MPa]	α_s [–]	g_{sMAX}: mmol/m^{2}s	LAI: m^2/m^2	H [m]	Z_r [cm]	d [mm]
Pinyon–Juniper	−2.8	−0.5	0.10	150	1.50	4.00	150	2.0
Larrea tridentata	−5.0	−0.4	0.15	180	0.50	1.00	40	1.5
Bouteloua gracilis	−4.0	−0.1	0.12	400	0.25	0.50	30	1.0
Bouteloua eriopoda	−4.5	−0.1	0.12	300	0.40	0.65	35	1.0

Ψ_w is the wilting-point matric potential, Ψ^* is the matric potential for incipient stomata closure, α_s is the shortwave albedo, g_{sMAX} is the maximum stomatal conductance, LAI is the leaf-area index, H is the average vegetation height, Z_r is the average root depth, and d is the canopy interception. Data for *Pinyon–Juniper*, *Larrea tridentata*, and *Bouteloua gracilis* are taken from a previous study of Rio Salado (1). *Bouteloua eriopoda* individuals are larger than *B. gracilis* ones (2). This fact has been taken into account by modifying the size parameters of *B. Eriopoda* (H and Z_r) as well as Ψ_w, g_{sMAX}, and LAI.

1. Caylor KK, Manfreda S, Rodriguez-Iturbe I (2005) On the coupled geomorphological and ecohydrological organization of river basins. *Adv Water Resour* 28:69–86.
2. US Department of Agriculture Service NRCS (2012) The PLANTS Database (National Plant Data Team, Greensboro, NC). Available at http://plants.usda.gov. Accessed June 2012.

Table S3. Soil parameters for the soil textures present in the basin

Soil type	Ψ_h [MPa]	Ψ_{sat} [MPa]	s_h [–]	s_{fc} [–]	K_s [cm/d]	n [–]	b [–]
Silt loam	−10.0	-5.55×10^{-3}	0.24	0.69	25.0	0.485	5.30
Loam	−10.0	-1.43×10^{-3}	0.19	0.54	20.0	0.451	5.39
Sandy loam	−10.0	-7.04×10^{-3}	0.14	0.44	80.0	0.435	4.90

Ψ_h is the hygroscopic point matric potential (1), Ψ_{sat} is the saturation point matric potential (1), s_h is the hygroscopic point relative soil moisture (1), s_{fc} is the relative soil moisture at field capacity (1), K_s is the saturated hydraulic conductivity (2), n is the porosity (1), and b is the pore distribution index (1).

1. Clapp RB, Hornberger GM (1978) Empirical equations for some soil hydraulic properties. *Water Resour Res* 14:601–604.
2. Laio F, Porporato A, Ridolfi L, Rodriguez-Iturbe I (2001) Plants in water-controlled ecosystems: Active role in hydrologic processes and response to water stress: II. Probabilistic soil moisture dynamics. *Adv Water Resour* 24:707–723.